IET Renewable Power Generation

Research Article

IET Journals
The Institution of Engineering and Technology

Bacteria foraging optimisation algorithm based optimal control for doubly-fed induction generator wind energy system

ISSN 1752-1416
Received on 8th February 2020
Revised 10th April 2020
Accepted on 28th April 2020
E-First on 3rd July 2020
doi: 10.1049/iet-rpg.2020.0172
www.ietdl.org

Hale Bakir[1,2], Adel Merabet[2] ✉, Rupak Kanti Dhar[2], Ahmet Afsin Kulaksiz[1]

[1]*Department of Electrical and Electronics Engineering, Konya Technical University, Konya, Turkey*
[2]*Division of Engineering, Saint Mary's University, 923 Robie Street, Halifax, NS B3H 3C3, Canada*
✉ *E-mail: adel.merabet@smu.ca*

Abstract: In this study, an optimisation method, based on bacteria foraging, is investigated to tune the parameters of the proportional–integral (PI) controllers in a doubly-fed induction generator (DFIG) wind energy system connected to the grid. The generator is connected to the grid directly at the stator and through the back-to-back converter at the rotor. The control system includes PI controllers, at the rotor side, to regulate the rotor currents and PI controller to regulate the dc-link voltage for efficient power transfer. The control parameters, of three PI controllers, are optimised offline using the bacteria foraging optimisation algorithm and a modelled DFIG wind energy system. Various performance criteria, based on the tracking errors, are used to assess the efficiency of the optimisation method. Furthermore, the conventional tuning method and genetic algorithm optimisation method are conducted and compared to the bacteria foraging optimisation method to demonstrate its advantages. The optimised control parameters are evaluated on a DFIG wind energy experimental setup. Experimental and simulation results are provided to validate the effectiveness of each optimisation method.

1 Introduction

Due to the rapid exhaustion of current energy sources, the increase in raw material prices, the negative effects on the environment and human health, and several difficulties in their use, the interest on new and renewable energy resources have increased. In addition, increasing energy consumption, awareness for environmental protection, and recent developments in energy production technologies stimulated interest in alternative energy and distributed production. Today, wind energy systems are among the principal providers of renewable energy due to their advantages such as high energy output and the ability of operation at variable speed. One of the most preferred wind generators is the doubly-fed induction generator (DFIG). The DFIG wind energy system allows producing energy with limited variable speeds that can operate with a speed difference of ±40% due to the high efficiency of the power converters [1].

In DFIG wind energy systems, the power converter unit has a back-to-back configuration of two converters called the rotor side converter (RSC) and the grid side converter (GSC). The RSC generates the required active and reactive power at the stator terminals by providing the required magnetisation current waveforms in the rotor windings [2]. Therefore, it ensures the control of the stator active and reactive power by controlling the rotor current components for maximum power extraction and desired power factor [3]. The GSC regulates the dc-link voltage and the grid current components for maximum power transfer from the rotor to the grid under the desired power factor. Furthermore, it can also be used to compensate for reactive power or to remove reactive power pulse under unstable conditions [2]. As multiple controllers are operating simultaneously, the performance of the DFIG wind energy system relies on the selection of the control parameters.

The vector control scheme, based on proportional–integral (PI) controllers, is a conventional method that is widely used in industrial applications due to its simplicity and good achievement of zero steady-state error. However, selecting the proportional and integral parameters is a challenging task and does not provide satisfactory results when using traditional adjustment and performance index methods as they are confronted with indeterminate dynamics, time delays and non-linearity. For this reason, researchers and engineers moved to intelligence optimisation algorithms for automatic control tuning.

The DFIG energy system, based on back-to-back power converters, is controlled using the vector control scheme, which includes PI controllers for the control loops (current and voltage–power). The performance of the DFIG system depends on the control parameters design [4]. Several studies have been dedicated to the optimisation of the PI control parameters for various DFIG systems. In [5], a bacterial foraging optimisation (BFO) algorithm is used to increase the damping of the oscillation modes of the DFIG system. The results of both eigenvalue analysis and time-domain simulation show that the damping controller set, in the DFIG system, is active. In [6], an optimal power flow solution for the IEEE 30-bus system is proposed. It has been found that the optimal solution obtained with a modified version of BFO yields better results than the genetic algorithm optimisation (GAO) based on the effect of wind and thermal timing on the total system cost. Furthermore, the superiority of the BFO method over ant colony optimisation (ACO) is revealed for an IEEE 30-bus system operating in a voltage-protected manner when exposed to certain conditions [7]. In [8], particle swarm optimisation (PSO) and BFO methods have been applied to design the parameters of PI–derivative (PID) control systems for the DFIG operation. Although the simulation results were satisfactory, the details in the algorithms, such as the selected cost function, were not provided in the implementation. Furthermore, it is not clear the purpose of using a PID instead of the PI configuration, which increases the computation time of the optimisation. In [9], an optimisation model with non-dominant sequencing genetic algorithm, based on the reference point, has been applied to the tune of the PI control parameters of a DFIG wind energy system. In [10], metaheuristic optimisation techniques, grey wolf optimiser (GWO) and artificial bee colony (ABC), have been applied for selecting the optimal parameters of the PI controllers for the control of the stator voltage and the current for a standalone DFIG energy system connected to a load. In [11], BFO has been employed to optimise the real power losses and voltage stability limit of a power network and compared with other methods, where it was concluded that BFO provides better results. In [12], a sensitivity analysis, to identify the critical control parameters, combined with PSO, to find the optimal values, has been applied to a DFIG wind generation system. The

© The Institution of Engineering and Technology 2020

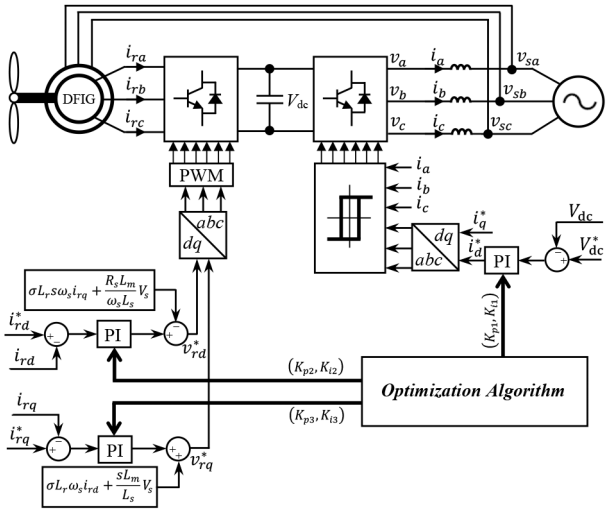

Fig. 1 *Control system for RSC and GSC of DFIG system*

sensitivity analysis reduces the optimisation complexity. A DFIG wind turbine system, with fault ride-through capability, has been studied in [13], using the PSO method for tuning the initial necessary stored energy in the superconducting coil and the PI control parameters of the dc–dc converter simultaneously. In [14], the parameters of a fractional-order sliding mode control, for the GSC of the DFIG, have been tuned using GAO for grid current and dc-link voltage control. Although it provides good tracking at the steady-state region, there are damped oscillations in the transient region. Furthermore, the control of the RSC and its effect are not discussed. In [15], the PSO method was used to optimise the coefficients of a subsynchronous resonance damping controller combined with vector control for power regulation of the DFIG energy system. However, the parameters of the PI controllers were selected by trial and error and the method was verified only by simulation.

In the above works, optimisation algorithms tune only the PI control parameters of the current controllers for the active–reactive power regulation without investigating the dc-link voltage regulation loop at the grid side. Furthermore, only a specific cost function has been used without any discussion about the choice of selection. In this study, the overall control system for the DFIG wind energy system will be studied, where the rotor currents at the RSC and the dc-link voltage at the GSC are controlled to operate the energy system. The BFO algorithm will be used to select the control parameters using different cost functions based on the tracking errors. In comparison to [8], a simpler cost function, in the swarming process, a PI control configuration and different preperformance indices will be used to alleviate the computational burden of the optimisation. Furthermore, the BFO results will be compared to the well-known artificial intelligence method based on GAO.

The remaining of the paper is organised as follows: the rotor side and grid side controllers for the DFIG-based wind system and the control system are explained in Section 2. BFO algorithm, for PI control parameter selection, is detailed in Section 3. Performance criteria for optimisation are provided in Section 4. Experimental and simulation results are analysed in Section 5. Finally, conclusions are addressed in Section 6.

2 DFIG wind energy system

2.1 Modelling

The DFIG wind energy system consists of a wind turbine, back-to-back converters, a resistive–inductive (*RL*) filter and a grid. The back-to-back converter configuration includes an RSC and a GSC. The system is depicted in Fig. 1.

At the DFIG rotor side, the rotor current dynamics is developed, in the synchronously rotating *d*–*q* reference frame, using the stator flux orientation, where the *q*-component of the stator voltage is aligned with the reference frame such as $v_{sd} = 0$ and $v_{sq} = V_s$. This dynamic is provided by the following expression [16, 17]:

$$\begin{cases} \dfrac{\mathrm{d}i_{rd}}{\mathrm{d}t} = -ai_{rd} + s\omega_s i_{rq} + \dfrac{R_s b}{\omega_s}V_s + \dfrac{1}{\sigma L_r}v_{rd} \\ \dfrac{\mathrm{d}i_{rq}}{\mathrm{d}t} = -ai_{rq} - s\omega_s i_{rd} - bsV_s + \dfrac{1}{\sigma L_r}v_{rq} \end{cases} \tag{1}$$

where $\sigma = 1 - (L_m^2/L_sL_r)$ is the leakage factor, $s = (\omega_s - \omega_r)/\omega_s$ is the slip, $a = (R_rL_s^2 + R_sL_m^2)/\sigma L_s^2L_r$, $b = L_m/\sigma L_sL_r$, R_s and R_r are the stator and the rotor resistances, respectively, L_s, L_r and L_m are the stator, the rotor and the mutual inductances, respectively, i_{rd} and i_{rq} are the *d*–*q* components of the rotor current, v_{rd} and v_{rq} are the *d*–*q* components of the rotor voltage, ω_s is the synchronous angular speed, ω_r is the rotor speed.

Using the rotor currents and the stator flux orientation, the active and reactive power of the DFIG stator side can be approximated by

$$\begin{cases} P_s = -\dfrac{3}{2}\dfrac{L_m}{L_s}V_s i_{rq} \\ Q_s = \dfrac{3}{2}\left(\dfrac{V_s\varphi_s}{L_s} - \dfrac{L_m}{L_s}V_s i_{rd}\right) \end{cases} \tag{2}$$

where φ_s is the stator flux.

It can be observed from the power (2), that the stator active power can be directly controlled through the *q*-component of the rotor current and the stator reactive power can be directly controlled through the *d*-component of the rotor current.

At the grid side, the current dynamics is given, in the *d*–*q* reference frame, by

$$\begin{cases} \dfrac{\mathrm{d}i_d}{\mathrm{d}t} = -\dfrac{R}{L}i_d + \omega i_q - \dfrac{V_s}{L} + \dfrac{1}{L}v_d \\ \dfrac{\mathrm{d}i_q}{\mathrm{d}t} = -\dfrac{R}{L}i_q - \omega i_d + \dfrac{1}{L}v_q \end{cases} \tag{3}$$

where R is the filter resistance, L is the filter inductance, respectively, i_d and i_q are the *d*–*q* components of the grid current, v_d and v_q are the *d*–*q* components of the grid converter voltage, which is also the DFIG stator voltage, and ω is the grid angular frequency.

At the grid side, the *d*-components of the vector control is synchronised such as $v_q = 0$. Therefore, the active power and reactive power at the grid side can be carried out by

$$\begin{cases} P_g = v_d i_d \\ Q_g = -v_d i_q \end{cases} \tag{4}$$

It can be observed from the power (4), that the grid active power can be directly controlled through the *d*-component of the grid current and the grid reactive power can be directly controlled through the *d*-component of the grid current.

The dc link, between the two converters, is governed by the dynamics expressed by [16–18]

$$\frac{\mathrm{d}V_{dc}}{\mathrm{d}t} = \frac{v_d}{CV_{dc}}i_d - \frac{1}{C}I_r \tag{5}$$

where V_{dc} is the dc-link voltage, C is the capacitance of the dc-link capacitor and I_r is the current from RSC. From the voltage dynamics (5), the dc-link voltage can be regulated by the *d*-component of the grid current to ensure proper transfer of the active power through the back-to-back converters.

2.2 Control system

The control system, at the GSC, consists of regulating the dc-link voltage through the outer control loop and regulating the grid

© The Institution of Engineering and Technology 2020

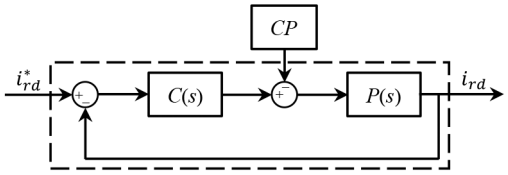

Fig. 2 *Configuration of the closed-loop system for i_{rd} dynamics*

currents through the inner control loop, as shown in Fig. 1. The outer control loop consists of a PI controller and provides the reference i^*_d. The inner control loop is based on the hysteresis controller.

The voltage control law, for the dynamics (5), is given by

$$i^*_d = K_{p1}e_v + K_{i1}\int e_v \,\mathrm{d}\tau \tag{6}$$

where $e_v = V^*_{\mathrm{dc}} - V_{\mathrm{dc}}$ is the voltage tracking error.

The control, at the RSC, consists on regulating the rotor currents, which allows controlling the active and reactive power of the DFIG stator as can be deduced from (2). The control law, derived from the state model (1), includes the PI controller and the compensation term such as

$$\begin{cases} v^*_{\mathrm{rd}} = K_{p2}e_d + K_{i2}\int e_d d\tau - \left(\sigma L_{\mathrm{r}} s\omega_{\mathrm{s}} i_{rq} + \dfrac{R_{\mathrm{s}}L_m}{\omega_{\mathrm{s}}L_{\mathrm{s}}}V_{\mathrm{s}}\right) \\ v^*_{\mathrm{rq}} = K_{p3}e_q + K_{i3}\int e_q d\tau + \left(\sigma L_{\mathrm{r}}\omega_{\mathrm{s}} i_{\mathrm{rd}} + \dfrac{sL_m}{L_{\mathrm{s}}}V_{\mathrm{s}}\right) \end{cases} \tag{7}$$

where $e_d = i^*_{\mathrm{rd}} - i_{\mathrm{rd}}$ and $e_q = i^*_{\mathrm{rq}} - i_{\mathrm{rq}}$ are the tracking errors for the d–q rotor currents, K_{p} and K_{i} are the proportional and the integral parameters, respectively, of the PI controllers.

2.3 Frequency-domain analysis

The frequency-domain design is a method to tune the parameters of the PI controller based on the transfer functions of the control and the system. The parameters values are carried out from the desired characteristics of the closed-loop system [18, 19].

For the concerned DFIG energy system, the design analysis can be applied to the dynamics (1) and (5). In this study, the design method is carried out for the rotor current i_{rd} and can be generalised for the other variables i_{rq} and V_{dc}.

From the rotor current dynamics (1), the closed-loop system, for i_{rd}, is illustrated in Fig. 2. The transfer functions, with respect of Laplace variable s, for the control $C(s)$ and the process $P(s)$ are given by

$$\begin{cases} C(s) = K_{\mathrm{p2}} + \dfrac{K_{\mathrm{i2}}}{s} \\ P(s) = \dfrac{1/\sigma L_{\mathrm{r}}}{(s+a)} \end{cases} \tag{8}$$

The compensation CP represents the decoupling with the q-component and is expressed by

$$CP = \sigma L_{\mathrm{r}} s\omega_{\mathrm{s}} i_{\mathrm{rq}} + \frac{R_{\mathrm{s}}L_{\mathrm{m}}}{\omega_{\mathrm{s}}L_{\mathrm{s}}}V_{\mathrm{s}} \tag{9}$$

In the frequency-domain design, the closed-loop system is based on the open-loop system $G(s) = C(s)P(s)$, as shown in Fig. 2, and has the expression

$$\frac{G(s)}{1+G(s)} \tag{10}$$

The function (10) has a second-order dynamics and its characteristics equation can be expressed under the form

$$s^2 + 2\xi\omega_n s + \omega_n^2 \tag{11}$$

where ξ is the damping coefficient and ω_n is the natural frequency.

The frequency-domain design consists on selecting the system roots by defining the coefficients ξ and ω_n and the performance of the step response. Then, these values are used in the calculation of the PI control parameters based on (10) and (11).

3 BFO algorithm

BFO algorithm has been inspired by the group foraging behaviour of bacteria like *E. coli*. The algorithm follows the chemotaxis behaviour of bacteria that move towards or away from the specific signals taking small steps while searching for food [20]. The foraging strategy is governed by four processes:

(i) *Chemotaxis*: This process is related to the movement of the bacterium that searches for food-rich location via flagella. When the searching is in the same direction of the previous step, it is called swimming and when the searching is in the opposite direction from the previous step, it is called tumbling.

The bacterium movement is defined by [20, 21]

$$P(i, j+1, k, l) = P(i, j, k, l) + C(i)\frac{\Delta(i)}{\sqrt{\Delta^T(i)\Delta(i)}} \tag{12}$$

where $P(i, j, k, l)$ is the ith bacterium at the jth chemotactic, the kth reproductive, and the lth elimination-dispersal step, $C(i)$ is the step size considered in a random direction, $\Delta(i)$ is a vector of random numbers, taken from [−1, 1], to represent an arbitrary direction. $\Delta(i)$ size depends on the optimisation problem.

(ii) *Swarming*: When an optimum path of food is reached by a bacterium, the other bacteria are attracted to reach the desired location by groups called swarms. The swarming is modelled by

$$J(i, j, k, l) = F(P(i, j, k, l)) \tag{13}$$

where J is the objective function, F is a function based on the optimisation problem, P is the parameter to be optimised.

(iii) *Reproduction*: In order to maintain a constant bacteria population, the healthy bacteria are divided into two bacteria in the same direction, to replace the dead unhealthy bacteria. The health of each bacterium during chemotaxis process is given by

$$J^i_{\mathrm{health}} = \sum_{j=1}^{N_c+1} J(i, j, k, l) \tag{14}$$

where J^i_{health} is the health of the ith bacterium and N_c is the chemotaxis step. In the sorting process, the higher cost means lower health.

(iv) *Elimination-dispersal*: Depending on a small probability, P_{ed}, some of the bacteria may die or move to another region (elimination) and new bacteria, for replacement, occur at a random point in the search space.

In this study, the aim is to optimise the PI control parameters $(\{K_{p1}, K_{i1}\}, \{K_{p2}, K_{i2}\}, \{K_{p3}, K_{i3}\})$ to minimise the tracking errors for the dc-link voltage V_{dc}, the d-axis rotor current i_{rd} and the q-axis rotor current i_{rq}, respectively. Therefore, the bacterium movement, defined in (12), is expressed using the following dimension of search space:

$$P(:, i, j, k, l) = \begin{bmatrix} P(1, i, j, k, l) \\ P(2, i, j, k, l) \\ P(3, i, j, k, l) \\ P(4, i, j, k, l) \\ P(5, i, j, k, l) \\ P(6, i, j, k, l) \end{bmatrix} = \begin{bmatrix} K_{p1} \\ K_{i1} \\ K_{p2} \\ K_{i2} \\ K_{p3} \\ K_{i3} \end{bmatrix} \tag{15}$$

The parameters P are subjected to bound constraints such as

© The Institution of Engineering and Technology 2020

$$l_b \le P \le u_b \tag{16}$$

where l_b and u_b are the lower bound and upper bound, respectively.

The function F, to be used in the objective function, will be defined based on a performance criterion related to the tracking errors as explained in the next section.

The algorithm of the bacteria foraging optimisation is described with details in the flowchart of Fig. 3. It includes three loops for elimination-dispersal, reproduction and chemotaxis processes of limits N_{ed}, N_{re}, and N_c, respectively. These processes are carried out for the S number of bacteria. The bacterium movement path P represents the optimised control parameters as described in (15). The objective function J is carried out using a performance criterion based on the tracking errors and the values of the optimised parameters as expressed in (13). The swimming occurs on a length of N_s. The reproduction is carried out, where the S_r unhealthy bacteria, based on the highest objective functions, die. In order to keep the bacteria group size the same as the original size S, copies are made and placed at the same location as their parents. This elimination-dispersal process is based on the probability P_{ed}. Finally, the best solution is selected from the minimum cost function and used to represent the values of the control parameters. The DFIG system is run with these values and the tracking errors are collected and compared to other methods to assess the performance of the BFO method.

4 Performance criteria for optimisation

In this study, integral of time-weighted absolute error (ITAE) has been used as a performance criterion for the optimisation algorithms and compared to the integral absolute error (IAE), the integral square error (ISE) and the integral time square error (ITSE). The comparison is performed to confirm the superiority of the ITAE.

Expressions of the performance criteria are given by

$$\text{IAE} = \int_0^\infty |e(t)|\,\mathrm{d}t \tag{17}$$

$$\text{ITAE} = \int_0^\infty t|e(t)|\,\mathrm{d}t \tag{18}$$

$$\text{ISE} = \int_0^\infty e^2(t)\,\mathrm{d}t \tag{19}$$

$$\text{ITSE} = \int_0^\infty t\,e^2(t)\,\mathrm{d}t \tag{20}$$

The optimisation goal is tuning the PI control parameters to minimise the tracking errors (e_v, e_d, e_q). The objective function is defined, using the ITAE criterion, such as

$$F(X) = \begin{bmatrix} \boldsymbol{w}_v & \boldsymbol{w}_d & \boldsymbol{w}_q \end{bmatrix} \begin{bmatrix} \int_0^T t|e_v|\mathrm{d}t \\ \int_0^T t|e_d|\mathrm{d}t \\ \int_0^T t|e_q|\mathrm{d}t \end{bmatrix} \tag{21}$$

where $\boldsymbol{X} = [K_{p1}, K_{i1}, K_{p2}, K_{i2}, K_{p3}, K_{i3}]^T$ is the vector of the control parameters, $\boldsymbol{w}_v$, $\boldsymbol{w}_d$ and $\boldsymbol{w}_q$ are the weighting factors.

5 Optimisation and results

The simulation and experimentation were conducted on the controlled DFIG-based wind energy system illustrated in Fig. 1. The experimental DFIG setup is depicted in Fig. 4. System parameters, for both simulation and experimentation, are given in Table 1.

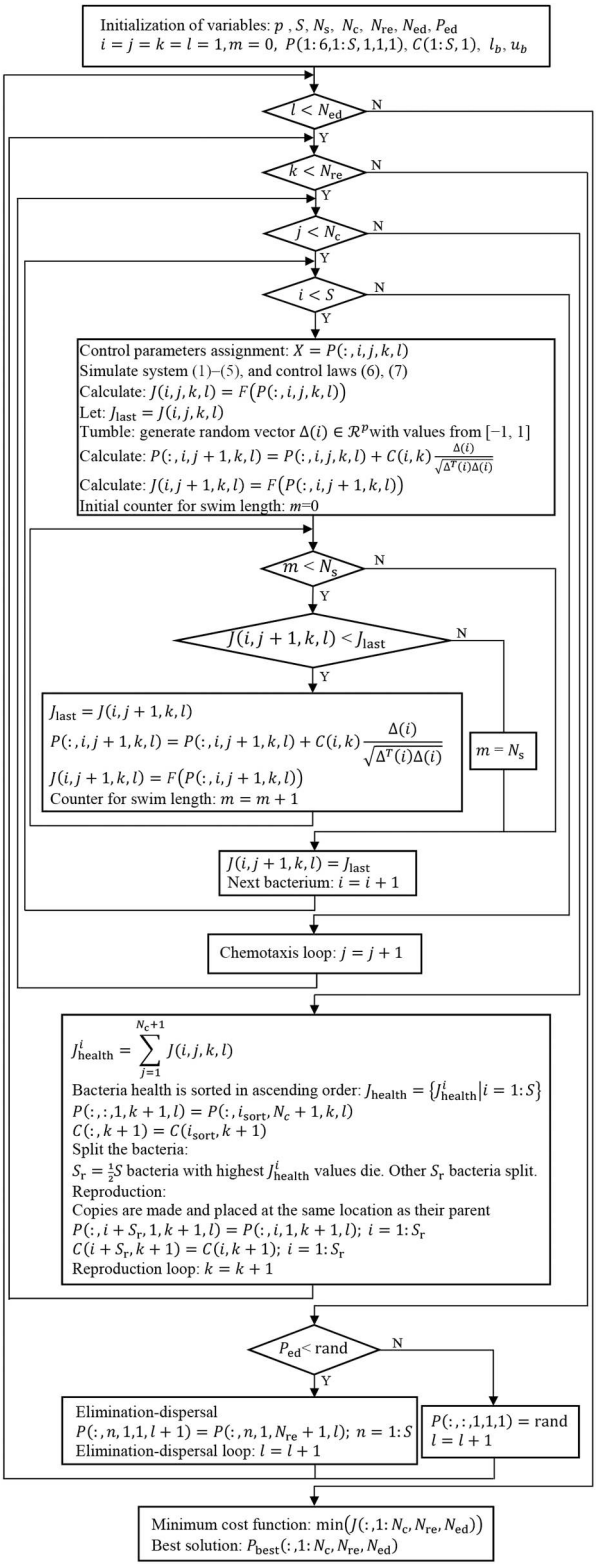

Fig. 3 *Flowchart of the BFO algorithm*

For the experimentation, a four-quadrant dynamometer was used to emulate the wind turbine. The OPAL-RT OP5600 was employed as the processor for the real-time control.

The data acquisition interface OP8660 was used to collect the measured voltages and currents of the DFIG system. Real-time simulation and hardware-in-the-loop are built in MATLAB/ Simulink and RT-Lab software environment.

5.1 Optimisation results

The six control parameters $[K_{p1}, K_{i1}, K_{p2}, K_{i2}, K_{p3}, K_{i3}]$ of the three PI controllers are optimised using conventional, GAO and BFO

© The Institution of Engineering and Technology 2020

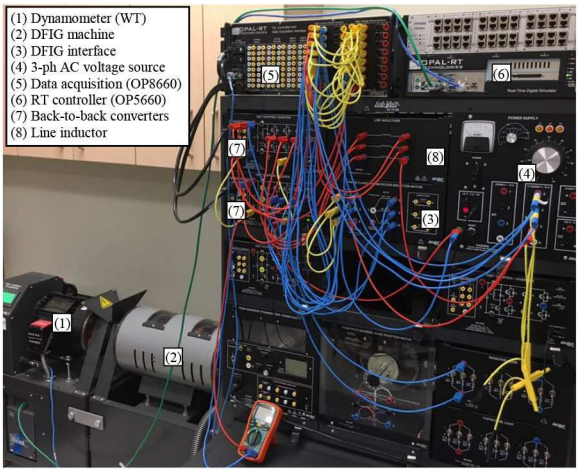

Fig. 4 *DFIG-based WECS experimental setup*

Table 1 DFIG parameters

Quantity	Symbol	Value
power	P_s	2 kW
stator voltage	V_s	120 V
rotor voltage	V_r	360 V
stator current	i_r	10 A
rotor current	i_s	3.3 A
nominal speed	ω_{nom}	1700 rpm
pole pairs	p	2
stator inductance	L_s	0.0662 H
rotor inductance	L_r	0.0662 H
mutual inductance	L_m	0.0945 H

Table 2 Computational time

	GAO	BFO
computation time, s	9020	6250

methods for the DFIG wind energy system. The optimisation was carried out using the performance indices IAE, ITAE, ISE, and ITSE, in the objective function (21). The purpose is showing the superiority of the ITAE over the other indices. The optimised values were deployed to regulate the dc-link voltage and d–q components of the rotor currents and operate the experimental setup.

The frequency-domain design, defined in Section 2.3, uses selected values of the damping coefficient, the natural frequency and the settling time for a step response. The control parameters are obtained using the expression [18]

$$\omega_n = \frac{4.6}{t_s * \xi} \tag{22}$$

$$K_p = \frac{2\xi\omega_n}{V_{max}} \tag{23}$$

$$K_i = \frac{\omega_n^2}{V_{max}} \tag{24}$$

where V_{max} is the maximum value of the voltage signal at the end of the busbar.

The selected values for a step response of the voltage and current controllers are $\xi = 0.707$, $t_s = 20$ ms and $V_{max} = 300$ V.

The BFO method has the following parameters:

1. dimension of search space: 6
2. iteration: 100
3. number of bacteria (S): 10
4. number of chemotactic steps (N_c): 5
5. limits the length of swim (N_s): 4
6. number of reproduction steps (N_{re}): 4
7. number of elimination-dispersal (N_{ed}): 2
8. probability for elimination/dispersion (P_{ed}): 0.25

The GAO method is implemented using the following parameters [2]:

1. population size: 10
2. selection: roulette wheel
3. cross-over rate: 0.8
4. mutation rate: 0.01
5. generations: 100
6. population type: double

The optimisation procedure is conducted off-line on the simulated DFIG wind energy system, depicted in Fig. 1, equivalent, in parameters, to the experimental setup. The simulation is carried out in MATLAB/Simulink environment.

At the start of the optimisation, the initial values of the parameters P in (15) are randomly selected with the bounds defined in (16). Any solution within the bounds (16) is considered suitable to operate the controlled DFIG system. Therefore, the optimal solution from the algorithm will always be within the bounds, which guarantees the convergence of the algorithm and the stability of the closed-loop system. After defining the parameters of the BFO, and using the initial values of the control parameters to operate the control system of the DFIG, the tracking errors (e_v, e_d, e_q) are carried out to calculate the objective function (21) to be used in (13). The BFO algorithm uses that objective function value to update the control parameters and repeats the sequence until reaching the stop condition as shown in the flowchart of Fig. 3.

The optimisation was conducted off-line using the processing unit Intel (R) Core (TM) i-5-3317U CPU@1.70 GHz. Computation time for GAO and BFO are provided in Table 2, where it can be observed that BFO requires less time, to provide the optimal solution, compared to the GAO for the same stop condition (iterations = 100).

The optimisation results for the GAO and BFO are provided in Table 3. It can be observed that the best and mean errors for the BFO are superior compared to the ones of the GAO for all performance criteria. Furthermore, the performance criterion ITAE provides the lowest best and mean errors compared to the other criteria as shown in Fig. 5. For this reason, the voltage and current controllers, in both simulation and experimentation, are assessed using the results of the optimisation methods based on the ITAE performance criterion. The optimised values, from the conventional, GAO and BFO with the ITAE performance criterion are used to run the simulation and operate the experimental DFIG wind energy system with the PI controllers for voltage and current regulation.

5.2 Simulation results

The controlled DFIG system, with optimised control parameters, is simulated for up-down step changes and the results are shown in Fig. 6. The DFIG is operational under constant rotor speed. It can be observed that dc-link voltage tracking, using the BFO, occurs with less overshoots at the transitions, as shown in Fig. 6*a*, compared to the conventional and GAO methods. For the d–q components of the rotor current, depicted in Figs. 6*b* and *c*, it can be observed the optimised control parameters by the three methods behave in a similar fashion with a slight advantage of the BFO method.

Now, in order to assess the dynamic performance at step response, the DFIG system is simulated, under constant rotor speed, using constant references for the dc-link voltage and the d–q components of the rotor current. The results are shown in Fig. 7 and the dynamic performance, based on the overshoot and settling

© The Institution of Engineering and Technology 2020

Table 3 Optimisation results

Performance index	PI control parameters	Genetic algorithm optimisation	Bacteria foraging optimisation
ITAE	dc-link voltage controller (K_{p1}, K_{i1})	0.8078, 0.3066	0.6424, 0.8781
	d-current controller (K_{p2}, K_{i2})	0.6689, 0.2795	0.6233, 0.8805
	q-current controller (K_{p3}, K_{i3})	0.9824, 0.2221	0.7518, 0.2045
	best	0.0703	0.06654
	mean	0.0721	0.068
ITSE	dc-link voltage controller (K_{p1}, K_{i1})	0.8945, 0.6806	0.7482, 0.1864
	d-current controller (K_{p2}, K_{i2})	0.7715, 0.7582	0.6791, 0.9532
	q-current controller (K_{p3}, K_{i3})	0.6762, 0.4691	0.9332, 0.1451
	best	1.5275	1.4338
	mean	1.5712	1.4791
IAE	dc-link voltage controller (K_{p1}, K_{i1})	0.8656, 0.7040	0.7687, 0.5431
	d-current controller (K_{p2}, K_{i2})	0.6662, 0.7220	0.2705, 0.0835
	q-current controller (K_{p3}, K_{i3})	0.8176, 0.2003	0.7117, 0.0199
	best	3.5214	3.3293
	mean	3.5358	3.3294
ISE	dc-link voltage controller (K_{p1}, K_{i1})	0.6797, 0.5853	0.8172, 0.5302
	d-current controller (K_{p2}, K_{i2})	0.4450, 0.3035	0.7299, 0.6729
	q-current controller (K_{p3}, K_{i3})	0.7572, 0.6299	0.7805, 0.1999
	best	355.527	340.513
	mean	355.531	340.568

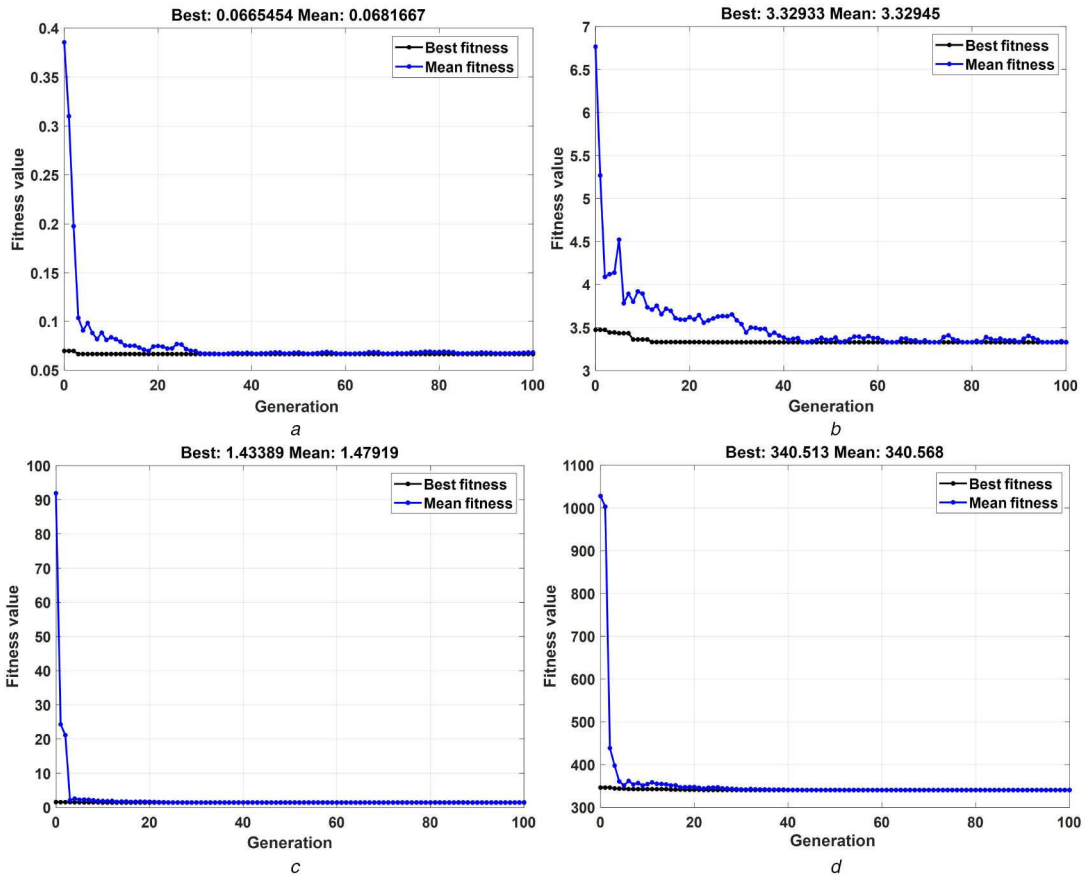

Fig. 5 *Convergence rates comparison for performance criteria*
(a) ITAE, ***(b)*** IAE, ***(c)*** ITSE, ***(d)*** ISE

times, for the three methods is provided in Table 4. From these results and the transient response dynamics, it can be observed that the optimised parameters using BFO provide better response compared to the conventional and the GAO methods.

In order to assess the performance of the controllers, optimised by the three methods, against turbulent wind speeds, the DFIG system was simulated under random speed variations. The dc-link voltage and *d*–*q* rotor currents are illustrated in Fig. 8, where it can be observed from the system responses that the dc-link voltage, shown in Fig. 8*a*, is well regulated, using the controllers optimised by BFO and GAO methods, compared to the conventional method, which is highly affected by the speed variations. However, the BFO shows better current tracking, for the *d*–*q* components of the rotor current shown in Figs. 8*b* and *b*, compared to the two other methods. From Fig. 8*c*, it can be observed that the *q*-current is

© The Institution of Engineering and Technology 2020

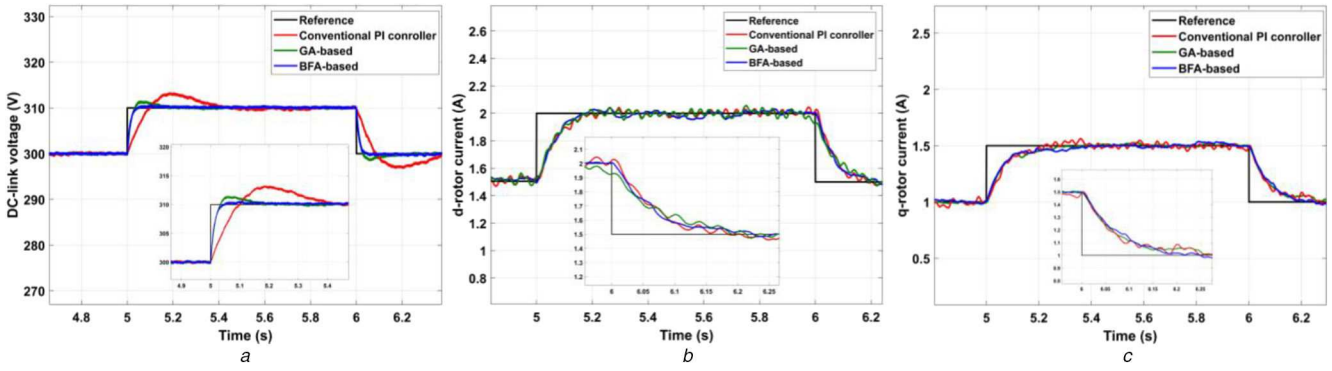

Fig. 6 *Control response under variable step references*
(a) dc-link voltage regulation, ***(b)*** *d*-rotor current regulation, ***(c)*** *q*-rotor current regulation

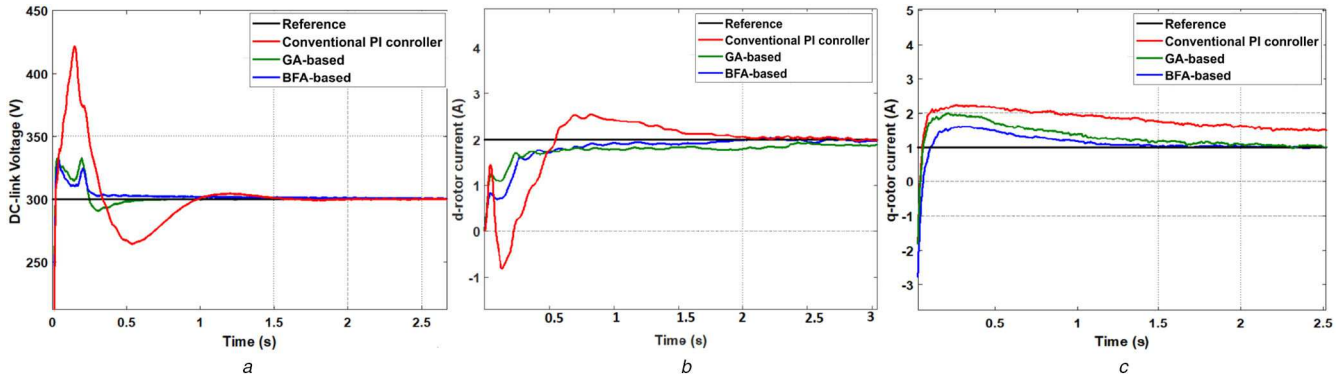

Fig. 7 *Control response under step references*
(a) dc-link voltage regulation, ***(b)*** *d*-rotor current regulation, ***(c)*** *q*-rotor current regulation

Table 4 Dynamic performance for simulation results

		Overshoot, %	Settling time, s	Peak values
dc-link voltage control	conventional	47.877	0.989	421.9
	GAO	25.776	0.329	337.6
	BFO	20.566	0.28	331.6
d-rotor current control	conventional	22.842	1.698	2.714
	GAO	3.777	2.28	2.128
	BFO	2.444	1.327	2.081
q-rotor current control	conventional	19.439	3.01	2.340
	GAO	18.383	1.527	2.054
	BFO	10.517	1.163	1.628

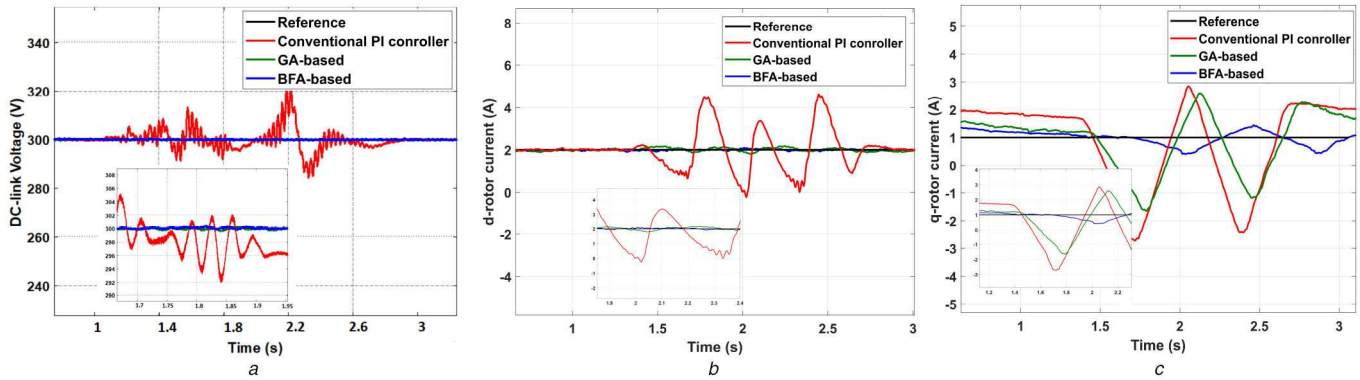

Fig. 8 *Control response under random rotor speed variations*
(a) dc-link voltage regulation, ***(b)*** *d*-rotor current regulation, ***(c)*** *q*-rotor current regulation

more affected by speed variations due to its influence on the torque generated by the DFIG against the rotor speed.

The total harmonic distortion (THD) analysis for the grid currents is shown in Fig. 9, where it can be observed that it is within the limits.

5.3 Experimental results

In all experiments, the optimised values, from the conventional, GAO and BFO with the ITAE performance criterion were used to operate the experimental DFIG wind energy system with the PI

© The Institution of Engineering and Technology 2020

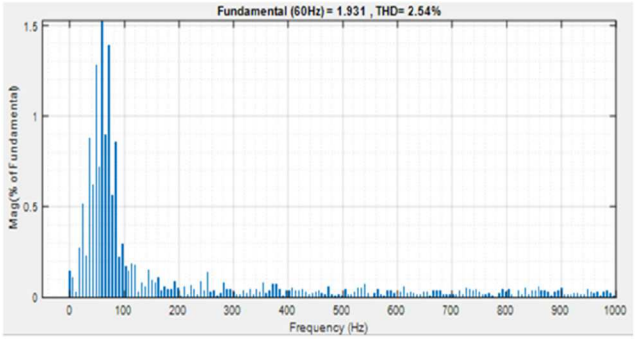

Fig. 9 *THD analysis for grid currents*

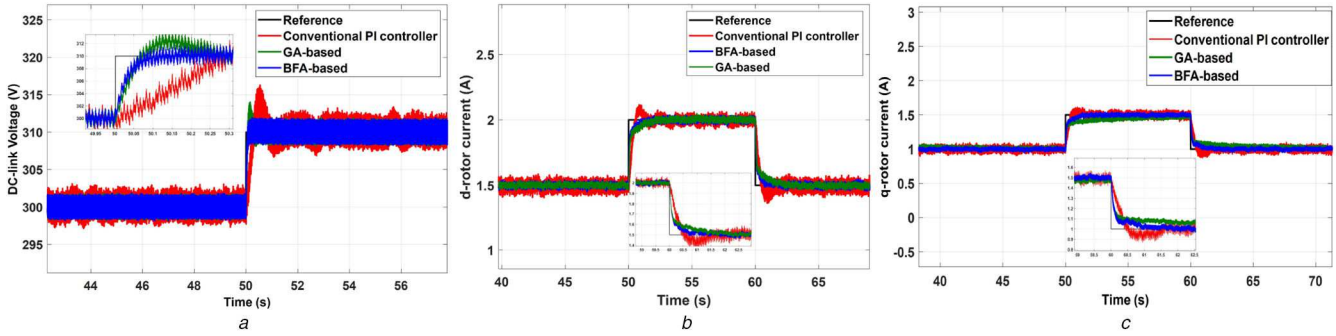

Fig. 10 *Control response under different optimisation methods*
(a) Step response for dc-link voltage, ***(b)*** Step response for *d*-rotor current, ***(c)*** Step response for *q*-rotor current

Table 5 Dynamic performance for experimental results

		Overshoot, %	Settling time, s	Peak values
dc-link voltage control	conventional	61.07	0.340	316.1
	GAO	30.05	0.240	313.4
	BFO	13.04	0.058	311.4
d-rotor current control	conventional	12.01	1.33	2.12
	GAO	2.025	1.18	2.025
	BFO	1.2	0.95	2.01
q-rotor current control	conventional	11.87	1.32	1.61
	GAO	3.02	1.05	1.53
	BFO	1.07	0.57	1.51

controllers for voltage and current regulation under the different conditions.

In the first experiment, the DFIG experimental setup was run under a constant rotor speed of 1650 rpm. The dc-link voltage reference was varied from 300 to 310 V at time $t = 50$ s and the d–q rotor current references were varied at time instants $t = 50$ s (step up) and $t = 60$ s (step down) to assess the control performance at the step transitions for the three optimisation methods. The experimental results for dc-link voltage and d–q components of the rotor currents are illustrated in Fig. 10. For the dc-link voltage response, shown in Fig. 10*a*, it can be observed that the settling time for the BFO-based control is less than the time of the control response based on conventional and GAO methods. Furthermore, there is no overshoot in the BFO-based tracking response compared to the two other methods. For the *d*-component of the rotor currents, depicted in Fig. 10*b*, it can be noticed that the BFO and GAO based controllers are faster in time response and have no overshoot compared to the conventional method. The same observation, on the time response, occurs at both transitions of the current reference (step up and step down). In addition, the BFO-based control is slightly faster than the GAO as can be seen in the zoom. For the *q*-component of the rotor currents, depicted in Fig. 10*c*, it can be noticed that the BFO based controller has better steady-state tracking error and the best settling time at both transitions. It is worth mentioning that the control parameters, optimised by GAO, provide much better tracking performance for the dc-link voltage and *d*-component of the rotor current compared to the conventional method in terms of the overshoot and settling time. These results are predictable as the conventional optimisation method is suitable for linear systems, which is not the case of the DFIG wind energy system, which includes compensation terms for the coupling dynamics. The dynamic time responses, for the step transition at 50 s in Fig. 10, are prented in Table 5, in which the superiority of the BFO compared to GAO and conventional methods, with respect of overshoot and settling time, can be observed.

Transient regimes, under fixed step references, are illustrated in Fig. 11. It is worth mention that the delays between the response are due to the running of the DFIG setup at different times as that startup is done manually. It can be observed from the results, for the dc-link voltage and d–q components of the rotor current, that optimised control parameters, using the BFO, provide better performance, with respect of overshoot and settling time, compared to the two other methods.

Now, the performance is verified against step variation in the rotor speed shown in Fig. 12*a*. The dc-link voltage regulation, shown in Fig. 12*b*, is well achieved using the control parameters optimised by BFO and GAO, whereas the response, using the conventional method, is affected by the variation of the rotor speed. The rotor currents are affected by the rotor speed variation with less effect on the current responses, shown in Figs. 12*c* and *d*, by the optimised control parameters using the BFO with respect of the overshoot and the settling time.

© The Institution of Engineering and Technology 2020

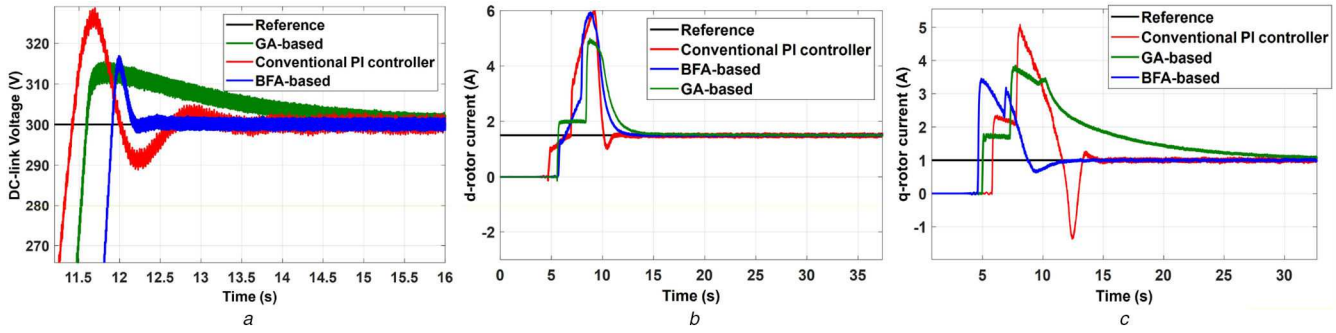

Fig. 11 *Transient region response under step references*
(a) dc-link voltage regulation, ***(b)*** *d*-rotor current regulation, ***(c)*** *q*-rotor current regulation

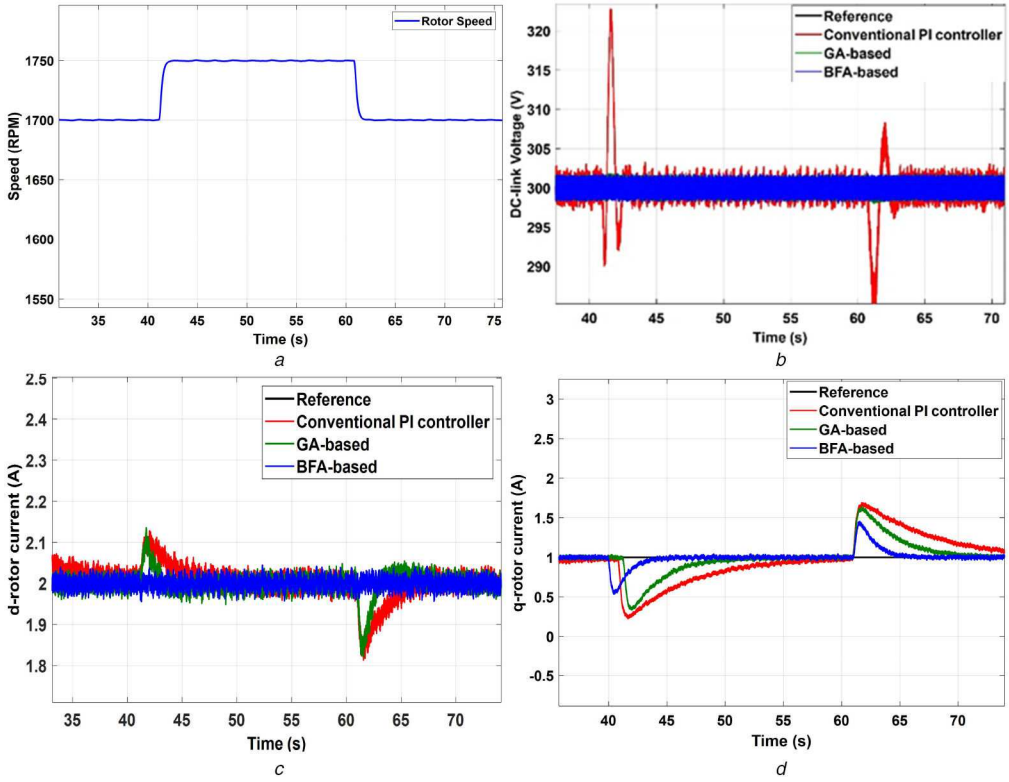

Fig. 12 *Control response under step changes in the rotor speed*
(a) Rotor speed profile, ***(b)*** dc-link voltage regulation, ***(c)*** *d*-rotor current regulation, ***(d)*** *q*-rotor current regulation

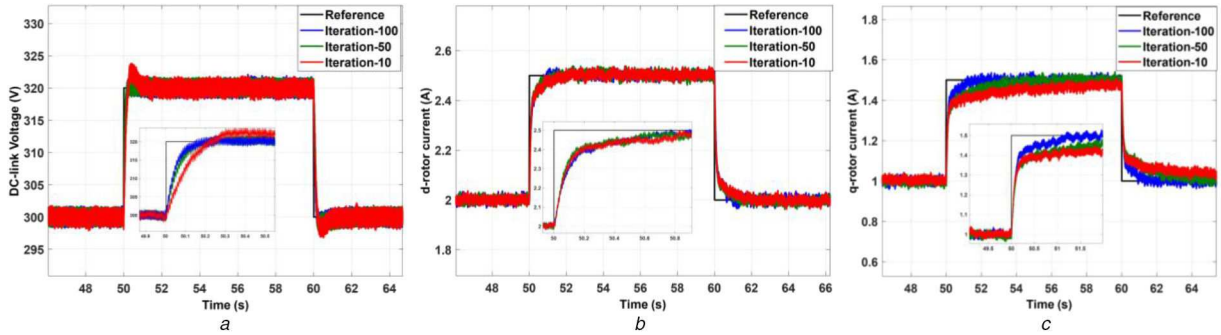

Fig. 13 *Control response for BFO under different iterations*
(a) dc-link voltage regulation, ***(b)*** *d*-rotor current regulation, ***(c)*** *q*-rotor current regulation

Finally, the BFO algorithm is assessed based on the number of iterations characterised by the bacteria population (S). The optimisation method was conducted for iterations 10, 50 and 100. The optimised values, based on each iteration, were used to operate the controllers in the DFIG energy system. The experimental results are illustrated in Fig. 13. Concerning the dc-link voltage regulation, shown in Fig. 13*a*, it can be observed that increasing the number of iterations reduces the overshoot and the settling time. For the d–q components of the rotor current, shown in Figs. 13*b* and *c*, more iterations indicate better tracking response. Therefore, the optimisation of the cost function is related to the number of iterations, where more iterations provides a minimum performance index. The drawback will be the increase in the execution time of the optimisation algorithm. Therefore, more studies are required to optimise the process.

© The Institution of Engineering and Technology 2020

Finally, it can be observed that the simulation results concur with the experimental results in showing the superiority of the BFO compared to conventional and GAO with respect of dynamic performance.

6 Conclusions

BFO algorithm was implemented to tune the parameters of PI controllers to operate an experimental DFIG wind energy system. The control objectives are to regulate the dc-link voltage and the rotor currents. The optimisation was carried out for six control parameters under different performance indices. The BFO method was compared to genetic algorithms and conventional frequency-domain design methods to show its advantage in ensuring zero steady-state errors with good performance. The advantage of the BFO, compared to the frequency-domain design, relies on the consideration of the compensation terms for the coupled dynamics of the DFIG system. The bacteria foraging algorithm is a powerful optimisation tool that can be used to tune the parameters or minimise the cost functions in optimal control applications.

7 Acknowledgments

This study was supported in part by the Scientific and Technological Research Council of Turkey (TUBITAK) BIDEB-2214 and the Canada Foundation for Innovation under grant no. 30527.

8 References

[1] Bakir, H., Kulaksiz, A.A.: 'Modelling and voltage control of the solar-wind hybrid micro-grid with optimized STATCOM using GA and BFA', *Eng. Sci. Technol. Int. J.*, 2020, **23**, (3), pp. 576–584

[2] Alhato, M.M., Bouallègue, S.: 'Direct power control optimization for doubly fed induction generator based wind turbine systems', *Math. Comput. Appl.*, 2019, **24**, (77), pp. 1–27

[3] Bansal, R.C., Bhatti, T.S., Kumar, V.: 'Reactive power control of autonomous wind-diesel hybrid power systems using ANN'. Proc. Int. Power Engineering Conf., Singapore, Singapore, 3–6 December 2007

[4] Zhou, D., Blaabjerg, F.: 'Bandwidth oriented proportional-integral controller design for back-to-back power converters in DFIG wind turbine system', *IET Renew. Power Gener.*, 2017, **11**, pp. 941–951

[5] Mishra, Y., Mishra, S., Tripathy, M.*, et al.*: 'Improving stability of a DFIG-based wind power system with tuned damping controller', *IEEE Trans. Energy Convers.*, 2009, **24**, (3), pp. 650–660

[6] Panda, A., Tripathy, M.: 'Optimal power flow solution of wind integrated power system using modified bacteria foraging algorithm', *Int. J. Electr. Power*, 2014, **54**, pp. 306–314

[7] Panda, A., Tripathy, M.: 'Security constrained optimal power flow solution of wind-thermal generation system using modified bacteria foraging algorithm', *Energy*, 2015, **93**, (1), pp. 816–827

[8] Bharti, O.P., Saket, R.K., Nagar, S.K.: 'Controller design of DFIG based wind turbine by using evolutionary soft computational techniques', *Eng. Technol. Appl. Sci. Res.*, 2017, **7**, (3), pp. 1732–1736

[9] Chen, A., Xie, D., Zhang, D.*, et al.*: 'PI parameter tuning of converters for sub-synchronous interactions existing in grid-connected DFIG wind turbines', *IEEE Trans. Power Electron.*, 2019, **34**, (7), pp. 6345–6355

[10] Soued, S., Chabani, M.S., Becherif, M.*, et al.*: 'Experimental behaviour analysis for optimally controlled standalone DFIG system', *IET Electr. Power Appl.*, 2019, **13**, (10), pp. 1462–1473

[11] Tripathy, M., Mishra, S.: 'Bacteria foraging-based solution to optimize both real power loss and voltage stability limit', *IEEE Trans. Power Syst.*, 2007, **22**, (1), pp. 240–248

[12] Tang, Y., Ju, P., He, H.*, et al.*: 'Optimized control of DFIG-based wind generation using sensitivity analysis and particle swarm optimization', *IEEE Trans. Smart Grid*, 2013, **4**, (1), pp. 509–520

[13] Karaipoom, T., Ngamroo, I.: 'Optimal superconducting coil integrated into DFIG wind turbine for fault ride through capability enhancement and output power fluctuation suppression', *IEEE Trans. Sustain. Energy*, 2015, **6**, (1), pp. 28–42

[14] Li, P., Xiong, L., Wang, Z.*, et al.*: 'Fractional-order sliding mode control for damping of subsynchronous control interaction in DFIG-based wind farms', *Wind Energy*, 2020, **23**, (3), pp. 749–762

[15] Yao, J., Wang, X., Li, J.*, et al.*: 'Sub-synchronous resonance damping control for series-compensated DFIG-based wind farm with improved particle swarm optimization algorithm', *IEEE Trans. Energy Conver.*, 2019, **34**, (2), pp. 849–859

[16] Tanvir, A., Merabet, A., Beguenane, R.: 'Real-time control of active and reactive power for doubly fed induction generator (DFIG)-based wind energy conversion system', *Energies*, 2015, **8**, pp. 10389–10408

[17] Merabet, A., Eshaft, H., Tanvir, A.: 'Power-current controller based sliding mode control for DFIG-wind energy conversion system', *IET Renew. Power Gener*, 2018, **12**, (10), pp. 1155–1163

[18] Teodorescu, R., Liserre, M., Rodriguez, P.: '*Grid converters for photovoltaic and wind power systems*' (Wiley-IEEE Press, UK, 2011)

[19] Madady, A.: 'Frequency domain approach to PI controller design for second order plus dead time processes'. Proc. 5th IEEE Int. Conf. Intelligent Systems, London, UK, 7–9 July 2010, pp. 1–6

[20] Passino, K.M.: 'Biomimicry of bacterial foraging for distributed optimization and control', *IEEE Control Syst. Mag.*, 2002, **22**, (3), pp. 52–67

[21] Chouhan, S.S., Kajul, A., Singh, U.P.*, et al.*: 'Bacterial foraging optimization based radial basis function neural network (BRBFNN) for identification and classification of plant leaf diseases: an automatic approach towards plant pathology', *IEEE Access*, 2018, **6**, pp. 8852–8863

© The Institution of Engineering and Technology 2020